Acquisition and Tracking of Starlink LEO Satellite Signals in Low SNR Regime

Haitham Kanj, Sharbel Kozhaya, and Zaher M. Kassas
The Ohio State University

BIOGRAPHY

Haitham Kanj is a Ph.D student in the Department of Electrical and Computer Engineering at The Ohio State University and a member of the Autonomous Systems Perception, Intelligence, and Navigation (ASPIN) Laboratory. He received a B.E. in Electrical Engineering from the Lebanese American University. His current research interests include opportunistic navigation, low Earth orbit (LEO) satellites, and cognitive software-defined radio. He is the recipient of the 2023 IEEE/ION Position, Location, and Navigation Symposium (PLANS) best student paper award.

Sharbel Kozhaya is a Ph.D student in the Department of Electrical and Computer Engineering at The Ohio State University and a member of the Autonomous Systems Perception, Intelligence, and Navigation (ASPIN) Laboratory. He received a B.E. in Electrical Engineering from the Lebanese American University. His current research interests include opportunistic navigation, low Earth orbit (LEO) satellites, cognitive software-defined radio, and 5G. He is the recipient of the 2023 IEEE/ION Position, Location, and Navigation Symposium (PLANS) best student paper award.

Zaher (Zak) M. Kassas is a professor at The Ohio State University and TRC Endowed Chair in Intelligent Transportation Systems. He is the Director of the Autonomous Systems Perception, Intelligence, and Navigation (ASPIN) Laboratory. He is also director of the U.S. Department of Transportation Center: CARMEN (Center for Automated Vehicle Research with Multimodal AssurEd Navigation), focusing on navigation resiliency and security of highly automated transportation systems. He received a B.E. in Electrical Engineering from the Lebanese American University, an M.S. in Electrical and Computer Engineering from The Ohio State University, and an M.S.E. in Aerospace Engineering and a Ph.D. in Electrical and Computer Engineering from The University of Texas at Austin. He is a recipient of the National Science Foundation (NSF) CAREER award, Office of Naval Research (ONR) Young Investigator Program (YIP) award, Air Force Office of Scientific Research (AFOSR) YIP award, IEEE Walter Fried Award, Institute of Navigation (ION) Samuel Burka Award, and ION Col. Thomas Thurlow Award. He is an Associate Editor of the IEEE Transactions on Aerospace and Electronic Systems and the IEEE Transactions on Intelligent Transportation Systems. He is a Fellow of the ION and a Distinguished Lecturer of the IEEE Aerospace and Electronic Systems Society. His research interests include cyber-physical systems, navigation systems, and intelligent transportation systems.

ABSTRACT

Acquisition and tracking of Starlink low Earth orbit (LEO) satellite signals in low signal-to-noise ratio (SNR) regime is considered. Starlink's highly dynamic downlink LEO signal model is derived, leading to coherence conditions for which the signals can be blindly tracked in low SNR regime. Next, the full-bandwidth Starlink beacon is estimated, and a time-bandwidth analysis of this beacon is presented. Finally, joint code and carrier phase Kalman filter-based loop is proposed for tracking Stralink LEO downlink signals in low SNR regime. Experimental results are presented showing successful Doppler tracking of 10 Starlink LEO satellites with a stationary receiver in low SNR regime. The Doppler observables were fused in a batch nonlinear least-squares estimator to yield a two-dimensional (2D) positioning error of 21.2 m, starting from an initial estimate 100 km away from the receiver's true position.

I. INTRODUCTION

Due to the known limitations of global navigation satellite systems (GNSS), there is an ever increasing interest in alternative positioning, navigation, and timing (PNT) systems. Literature over the past decade explored the use of ambient terrestrial radio frequency signals of opportunity (SOPs) for PNT (Raquet *et al.*, 2021; Souli et al., 2022; Fokin and Volgushev, 2022). Examples of terrestrial SOPs exploited for PNT include: (i) AM/FM radio (Chen et al. (2020)), (ii) cellular (e.g., 3G (Khalife et al. (2016)), 4G (Tian et al. (2023)), and 5G (del Peral-Rosado et al. (2022)), and (iii) digital television (Jiao et al., 2023).

The birth of low Earth orbit (LEO) satellite megaconstellations has resulted in tremendous interest in exploring the use of their signals for PNT (Kassas et al., 2019; Jardak and Jault, 2022; Prol et al., 2022; Janssen et al., 2023; Menzione and Paonni, 2023; Prol et al., 2023). Numerous studies have been published over the past few years addressing various challenges in opportunistic PNT with LEO, from addressing space vehicle (SV) orbit, clock, and propagation errors (Mortlock and Kassas, 2021; Morton et al., 2022; Cassel et al., 2022; Wang et al., 2023; Zhao et al., 2023; Wu et al., 2023; Jiang et al., 2023; Ye et al., 2023; Saroufim

et al., 2023); receiver and signal design (Tan et al., 2019; Wei et al., 2020; Bilardi, 2021; Kassas et al., 2021; Egea-Roca et al., 2022; Huang et al., 2022; Pinell et al., 2023; Yang et al., 2023); and analyzing the estimation performance (Farhangian et al., 2021; Hartnett, 2022; Singh et al., 2022; Jiang et al., 2022; More et al., 2022; Shi et al., 2023; Guo et al., 2023; Kanamori et al., 2023; Sabbagh and Kassas, 2023).

Whenever the LEO downlink signal structure is sufficiently known, designing a receiver that could acquire and track such signals becomes a "classic" receiver design problem. Examples of LEO constellations with sufficient knowledge about their downlink signal include Orbcomm and Iridium. Nevertheless, new LEO megaconstellations, such as Starlink and OneWeb, do not disclose public information about their signals. This challenge can be addressed with blind signal processing techniques. Previous research was capable of estimating downlink sequences in direct sequence spread spectrum communication systems (Tsatsanis and Giannakis, 1997; Burel and Bouder, 2000; Choi and Moon, 2020; Li et al., 2023), for GPS/GNSS signals under non-cooperative conditions (Merwe et al., 2020; Rui et al., 2022), and for orthogonal frequency-division multiplexing (OFDM) signals (Bolcskei, 2001; Tanda, 2004; Liu et al., 2010). In the context of LEO, (Neinavaie et al., 2021; Kozhaya and Kassas, 2022) developed blind Doppler tracking approaches for Obrcomm LEO SVs; while (Khalife et al., 2022) was the first to successfully apply blind signal processing techniques on Starlink LEO signals, yielding carrier phase observables, from which a stationary receiver was localized with a two-dimensional (2D) error of 25.9 m with signals from six Starlink LEO SVs. Another blind approach, based on matched subspace detection, was developed in (Neinavaie et al., 2022; Neinavaie and Kassas, 2023b), yielding Doppler observables, from which a stationary receiver was localized with a 2D error of 10 m (with pure tones) and 6.5 m (with OFDM signals in addition to pure tones) from the same six Starlink LEO SVs. A blind spectral-based approach was developed in (Kozhaya and Kassas, 2023), yielding Doppler observables, from which a stationary receiver was localized with a 2D error of 4.3 m with the same six Starlink LEO SVs. In (Kozhaya et al., 2023; Kassas et al., 2023), it was demonstrated that this approach is rather general, referred to as LEO-agnostic, and is capable of acquiring and tracking LEO signals regardless of their modulation and multiple access schemes. In addition to Starlink LEO, the approach was successfully applied to OneWeb, Orbcomm, and Iridium LEO SVs, yielding Hz-level-accurate Doppler tracking, from which a stationary receiver was localized with a 2D error of 5.1 m with 2 OneWeb, 4 Starlink, 1 Iridium, and 1 Orbcomm LEO SVs. Starlink's OFDM signal structure was later disclosed in (Humphreys et al., 2023), while (Yang and Soloviev, 2023; Jardak and Adam, 2023) studied tracking of Starlink's pure tones with a low-noise block (LNB) and (Stock et al., 2023) analyzed the Starlink user uplink signals for PNT.

In general, the fact that LEO SVs are closer to Earth implies a higher received signal-to-noise ratio (SNR). However, new LEO constellations, such as Starlink, employ phased antenna arrays (Chi et al., 2023) to beamform their signals toward their *subscribing* users (Neinavaie and Kassas, 2022, 2023a). As such, the SNR is only high whenever an *opportunistic* receiver is in the vicinity of an active user terminal. This phenomenon was witnessed whenever the previously designed blind algorithms (Neinavaie and Kassas, 2023b; Kozhaya and Kassas, 2023), which successfully tracked Starlink LEO signals in Southern California, USA, in which active Starlink user terminals were nearby; failed to track Starlink signals in Columbus, Ohio, USA, which, at the time of performing the experiments, was not within Starlink's coverage. This paper addresses the challenge of tracking LEO SVs in low SNR regime, from which navigation observables can be generated. To the author's knowledge, this challenge has not been addressed yet in the literature.

This paper focuses makes the following contributions: (i) derives the conditions under which Starlink's downlink LEO signals can be blindly tracked in low SNR regime, (ii) presents a time-bandwidth analysis of the estimated downlink beacon, (iii) designs a joint code and carrier phase Kalman filter (KF)-based tracking loop capable of tracking LEO SVs in low SNR regime, and (iv) presents experimental results of 10 Starlink LEO SVs tracked in low SNR regime, from which a stationary receiver was localized with a 2D error of 21.2 m, starting from an initial estimate 100 km away from the receiver's true position.

The paper is organized as follows. Section II derives the signal model. Section III presents the Starlink blind beacon estimation framework. Section IV presents the proposed signal acquisition and tracking approach. Section V shows the experimental tracking and positioning results in low SNR regime. Section VI gives concluding remarks.

II. SIGNAL MODEL

This section derives the received signal model under assumptions associated with a highly dynamic channel between a LEO SV and a ground based opportunistic receiver. This paper assumes the existence of repetitive sequences in the downlink LEO SV signal. Almost all communication channels require a periodic sequence referred to as the beacon. Examples of such periodic sequences are: (i) pseudorandom noise codes used in spread spectrum code division multiple access (CDMA) systems like cellular 3G (3GPP2 (2011)), GPS (Navstar GPS (2015)), and Globalstar LEO Hendrickson (1997), and (ii) the primary synchronization block utilized in OFDM modulation in cellular 4G (3GPP (2010)) and cellular 5G (3GPP (2018)). Let $s(t)$ and $m(t)$ denote the beacon with period T_{sub} and the user data sent by a LEO SV, respectively. This paper assumes that these two signal components are uncorrelated. Define, $x(t) \triangleq s(t) + m(t)$ as the transmitted LEO signal which becomes $x_c(t) \triangleq x(t)\exp(j2\pi f_c t)$ after carrier modulation, where f_c is the carrier frequency. Define the variables $\delta_{LOS}(t)$ as the line-of-sight time-of-flight between the LEO SV and the opportunistic receiver, $\delta_{atm}(t)$ as the atmospheric delay the transmitted

signal experiences as a result of propagating through the ionosphere and troposphere, and $\delta_{clk}(t)$ as the clock mismatch between the LEO SV and the opportunistic receiver. Now, define $\tau(t) \triangleq \delta_{LOS}(t) + \delta_{atm}(t) + \delta_{clk}(t)$ as the apparent delay observed at the receiver. Therefore, the received signal before carrier wipe-off can be expressed as

$$\begin{aligned} r_c(t) &\triangleq x_c\left(t-\tau(t)\right) + n_c(t) \\ &= x(t-\tau(t)) \exp\left[\, j2\pi f_c \left[t-\tau\left(t\right)\right]\right] + n_c(t). \end{aligned} \tag{1}$$

$x(t)$ captures the channel noise, which is modeled as a complex Gaussian white random process with power spectral density of $\frac{N_0}{2}$. After carrier wipe-off and filtering, the received base-band signal is expressed as

$$\begin{aligned} r_b(t) &\triangleq r_c(t) \exp\left[\, -j2\pi(f_c - f_e)t\right] \\ &= x(t-\tau(t)) \exp\{j\left[\, \theta(t) + 2\pi f_e t\right]\} + n_b(t), \end{aligned}$$

where f_e is the frequency error of the LNB down-converter, $\theta(t) \triangleq -2\pi f_c \tau(t)$ and $n_b(t)$ is the base-band low-pass filtered version of $n_c(t)$. Note that because a commercial LNB utilizes a temperature-compensated crystal oscillator (TCXO) with expected error in the $\left[0, 30\right]$ kHz range and the clock is not disciplined to GNSS, f_e cannot be ignored. Define the support function $w_{T_{sub}}(t)$ as

$$w_{T_{sub}}(t) \triangleq \begin{cases} 1, & t \in [0, T_{sub}) \\ 0, & \text{otherwise.} \end{cases}$$

In this paper, $\theta_k(t) \triangleq \theta(t) w_{T_{sub}}(t - t_k)$ is approximated by its second order Taylor series expansion (TSE) at time instant $t_k = t_0 + kT_{sub}$, where t_0 is some initial time, and k is the sub-accumulation index, according to

$$\begin{aligned} \theta_k(t) &\approx \theta_0(t_k) + \dot{\theta}(t_k)(t-t_k) + \frac{1}{2}\ddot{\theta}(t_k)(t-t_k)^2 \\ &= \theta_0(t_k) + f_D(t_k)(t-t_k) + \frac{1}{2}\dot{f}_D(t_k)(t-t_k)^2, \end{aligned} \tag{2}$$

where $f_D(t)$ is the apparent Doppler shift, $\dot{f}_D(t)$ is the apparent Doppler rate, and $t \in [0, T_{sub})$. Equivalently, $\tau(t)$ can be expressed as

$$\tau_k(t) \approx \tau_0(t_k) + \dot{\tau}(t_k)(t-t_k) + \frac{1}{2}\ddot{\tau}(t_k)(t-t_k)^2. \tag{3}$$

Furthermore, the received signal $r_k^*(t)$ before carrier phase wipe-off using the carrier phase estimate denoted $\hat{\theta}_k(t)$ generated by the tracking loop discussed in Section IV at the k-th sub-accumulation can be expressed as

$$\begin{aligned} r_k^*(t) &\triangleq r_b(t) w_{T_{sub}}(t - t_k) \\ &= s_k(t) \exp\left\{j\left[\theta_k(t) + 2\pi f_e t\right]\right\} + n_k^*(t), \end{aligned} \tag{4}$$

where $s_k(t) \triangleq s(t - \tau_k(t)) w_{T_{sub}}(t)$ and the term $n_k^*(t) \triangleq \left[n_b(t-\tau_k(t)) + m(t-\tau_k(t))\right] w_{T_{sub}}(t)$ represents the lumped user data and channel noise. The received signal $r_k(t)$ after carrier wipe-off using the carrier phase estimate, denoted $\hat{\theta}_k(t)$, generated by the tracking loop discussed in Section IV, can be expressed as

$$\begin{aligned} r_k(t) &= r_k^*(t) \exp\{-j\left[\hat{\theta}_k(t) + 2\pi \hat{f}_e t\right]\} \\ &= s_k(t) \exp\left[\, j\tilde{\theta}_k(t)\right] + n_k(t), \end{aligned} \tag{5}$$

where $\tilde{\theta}_k(t) = \theta_k(t) - \hat{\theta}_k(t) + 2\pi(f_e - \hat{f}_e)t$ is the residual carrier phase and $\hat{f}_e$ is the Doppler ambiguity estimate of the LNB clock error generated in Section IV.

III. STARLINK DOWNLINK BEACON ESTIMATION

This section presents the beacon estimation framework used to estimate Starlink LEO SV's downlink beacon. Next it analyzes the time-frequency characteristics of this beacon.

1. Signal Capture Setup

This subsection presents the blind beacon estimation framework to estimate the repetitive sequence in Starlink's LEO downlink signals. For this purpose, a high-gain signal capture setup was used (see Figure 1). An LNB with 2.5 dB noise figure is mounted on a 30 dBi Ku-Band parabolic antenna to collect high SNR Starlink signals. The RF signal is then fed into a stationary National Instrument (NI) universal software radio peripheral (USRP) X-410 whose sampling frequency was set to 500 MHz. This allows for estimation of the full bandwidth beacon of Starlink which spans 240 MHz. The total experiment duration was 60 seconds.

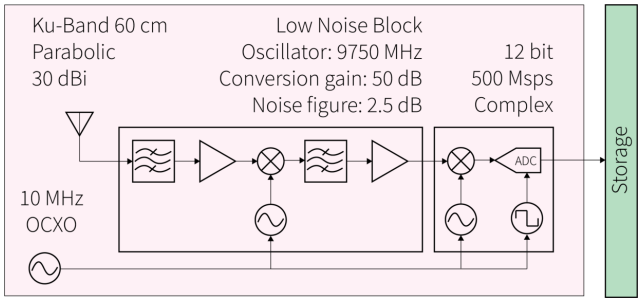

Figure 1: Block diagram of high-gain Starlink signal capture setup.

2. Blind Beacon Estimation

The continuous-time signal in (4) was sampled at a constant sampling interval $T_s = 1/F_s$. The discrete-time received signal before carrier wipe-off at the k-th sub-accumulation can be written as

$$r_k^*[n] = s[n - d_k[n]] \exp\left(j\Theta_k[n]\right) + n_k^*[n], \tag{6}$$

where $n \in [0, L-1]$; $s[n]$ is the discrete-time equivalent of $s(t)$ with period $L = T_{sub}/T_s$; $\Theta_k[n]$ and d_k are the discrete-time carrier phase and code phase, respectively, of the received signal at the k-th sub-accumulation; and $n_k^*[n]$ is the discrete-time equivalent of $n_k^*(t)$. Note that $\Theta_k[n]$ is made to include the effects of the frequency clock error f_e for ease of further analysis. Let M denote the number of sub-accumulations used per accumulation. In order to maintain carrier phase coherence in any correlation-based receiver over the accumulation interval, the following condition must be satisfied

$$2\tilde{f}_D M T_{sub} + \tilde{\dot{f}}_D (M T_{sub})^2 \ll \frac{1}{2}, \tag{7}$$

where $\tilde{f}_D$ and $\tilde{\dot{f}}_D$ are the errors associated with the estimates of the Doppler f_D and Doppler rate $\dot{f}_D$. Also, to maintain code phase coherence over the accumulation interval, the following condition must be satisfied

$$\tilde{\dot{\tau}} M T_{sub} + \tilde{\ddot{\tau}} (M T_{sub})^2 \ll \frac{1}{F_s}, \tag{8}$$

where $\tilde{\dot{\tau}}$ and $\tilde{\ddot{\tau}}$ are the errors associated with the estimates of the code phase rate $\dot{\tau}$ and code phase acceleration $\ddot{\tau}$. Knowing that the maximum realized Doppler rate for Starlink is $\dot{f}_D \approx 3$ kHz and that $\ddot{\tau} = \frac{-\dot{f}_D}{F_c}$, it can be seen that the maximum error $\tilde{\ddot{\tau}} \approx 0.27\,\mu\text{s/s}^2$. Therefore, for a reasonable choice of number of sub-accumulations M, $\ddot{\tau}$ can be ignored and (8) simplifies to $\tilde{\dot{\tau}} M T_{sub} F_s \ll 1$.

The first step in beacon estimation is verifying the existence of a repetitive sequence. Figure 2 shows the normalized auto-correlation profile of a 100 ms window of the collected signal. The repetitive peaks with spacing T_{sub} = 4/3 ms validates the existence of the repetitive sequence. Furthermore, in the beacon estimation stage, choosing M = 1 is sufficient given the high signal to noise ratio (SNR) of the collected signal. Let T denote the total number of accumulations used for beacon estimation, which was chosen to be 70 herein. Given these choice of T and M under the conditions (7) and (8), the blind beacon estimator should be able to resolve for the relative carrier phase shift, Doppler shift, and code phase shift between the different accumulations.

Let $\boldsymbol{r}_k$ denote the complex vector form of (6) such that

$$\boldsymbol{r}_k \triangleq \left[r_k^*[0], \ldots, r_k^*[L-1]\right], \quad \boldsymbol{y} \triangleq \left[\boldsymbol{r}_1^\mathsf{T}, \ldots, \boldsymbol{r}_T^\mathsf{T}\right],$$

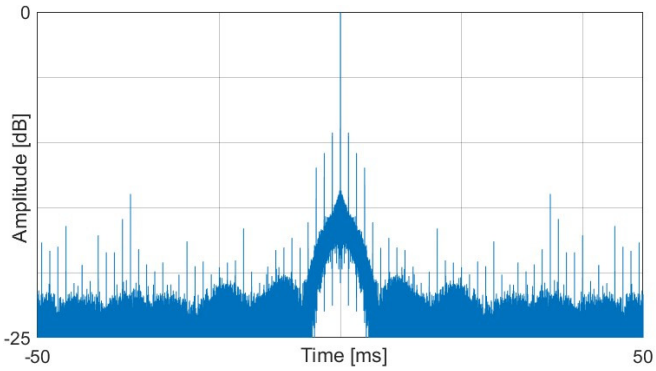

Figure 2: Normalized auto-correlation of a 100 ms window of Starlink's received signal.

Algorithm 1 Beacon Estimation Algorithm

Input $\mathbf{y},\ T_s,\ \gamma$
Output $\hat{\mathbf{s}}$

$\hat{\mathbf{s}} \leftarrow \mathbf{y}[0],\ w \leftarrow 0$
for $k = \{1, \ldots, T-1\}$ **do**
  $[\Delta\hat{d}_k, \Delta\hat{f}_D] = \text{argmax}_{d,\Delta f_D} \left| \left(\hat{\mathbf{s}} \star \boldsymbol{r}_k^{\mathsf{T}} \exp[j2\pi\Delta f_D n T_s]\right)[d] \right|^2$
  $R = \left(\hat{\mathbf{s}} \star \boldsymbol{r}_k^{\mathsf{T}} \exp[j2\pi\Delta\hat{f}_D n T_s]\right)[\Delta\hat{d}_k]$
  if $|R| > \gamma$ **then**
    $w \leftarrow w + 1$
    $\hat{\mathbf{s}} \leftarrow \frac{w}{w+1}\hat{\mathbf{s}} + \frac{1}{w+1}\text{circshift}\left(\boldsymbol{r}_k^{\mathsf{T}}, \Delta\hat{d}_k\right) \exp[j(2\pi\Delta f_D n T_s + \angle R)]$
  else
    continue
  end if
end for

where $\boldsymbol{y}$ is a matrix containing all T sub-accumulations of the received signal described in (6) that will be used for beacon estimation. Next, the beacon estimation algorithm is performed according to Algorithm 1. First, the initial accumulation is taken as a reference signal. Second, the reference signal is correlated with the next available accumulation in search for the best estimates of the relative code phase shift $\Delta\hat{d}_k$ and relative Doppler shift $\Delta\hat{f}_D$, which maximize the correlation between the beacon estimate $\hat{\boldsymbol{s}}$ and the current available accumulation. Note that this method works only under the assumption of high SNR data, i.e. the correlation between two consecutive accumulations is capable of producing a prominent peak. Let,

$$(\mathbf{s} \star \mathbf{r})[d] = \sum_{n=1}^{L} \mathbf{s}^*[n]\mathbf{r}\left[\text{mod}(n+d, L)\right],$$

denote the discrete-time circular cross-correlation of $\boldsymbol{s}$ and $\boldsymbol{r}$ where $\text{mod}(\cdot,\cdot)$ denotes the modulo operator. Next, if the magnitude of the correlation passes the predetermined threshold γ, the beacon estimate is updated using the estimates $\Delta\hat{d}_k$, $\Delta\hat{f}_D$, and the current accumulation. This process is repeated until the all the M accumulations are used, and then the beacon estimation process is complete. Note that because the algorithm relies on initializing the reference signal as an arbitrary accumulation, the resulting beacon contains a Doppler ambiguity. However, this carrier phase ambiguity can be resolved by tracking an arbitrary Starlink SV Doppler using the tracking loops in Section IV. After that, for beacon estimation purposes only, the position of the receiver is used to generate the expected Doppler measurements from the TLE + SGP4, and then the Doppler ambiguity would be the Doppler shift that would minimize the total error between the measured Doppler and estimated Doppler from TLE + SGP4.

3. Beacon Analysis

This section analyzes the Starlink LEO beacon in the downlink channel. Figure 3 shows the amplitude of 40 ms of the high SNR Starlink LEO downlink signal. It is observed that the downlink signal is non-stationary with varying power levels, even between two consecutive sub-accumulation intervals. This highlights the importance of (i) increasing the number of sub-accumulations

used, M, for any correlation-based receiver to increase the probability of getting higher power frames per accumulation, and (ii) the threshold γ defined in the beacon estimation stage which prevents low power sub-accumulations from skewing the beacon estimate. The auto-correlation profile of the beacon versus signal bandwidth is shown in Figure 4. As expected, the auto-correlation profile peak width decreases as the bandwidth of the beacon increases to reach the full bandwidth at 240 MHz. However, under condition (8), it is most favorable to choose the lowest F_s sufficient for acquisition and tracking purposes. Furthemore, let $R_x[d] = (x \star x)[d]$ denote the discrete circular auto-correlation function. It is also observed that for an F_s of 2.5 MHz, $\angle R_x[1] \approx \angle R_x[0] + \pi$ and $|R_x[1]| \approx 0.33\,|R_x[0]|$. This implies that a large choice of M results in worse correlations in the absence of code phase rate compensation. This amplifies the importance of satisfying condition (8) for code phase coherence.

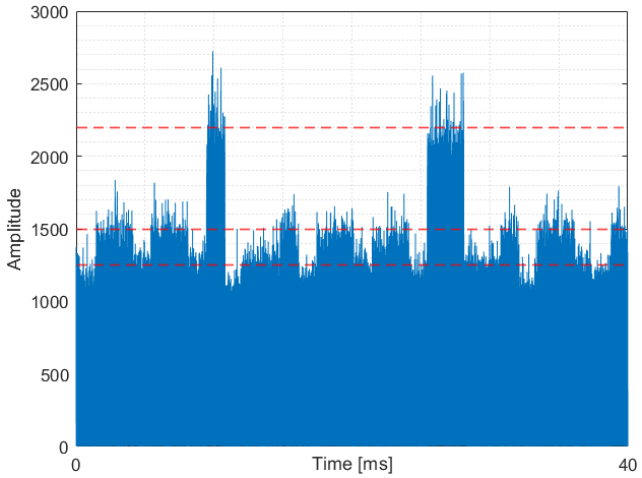

Figure 3: Amplitude of 40 ms of received signal.

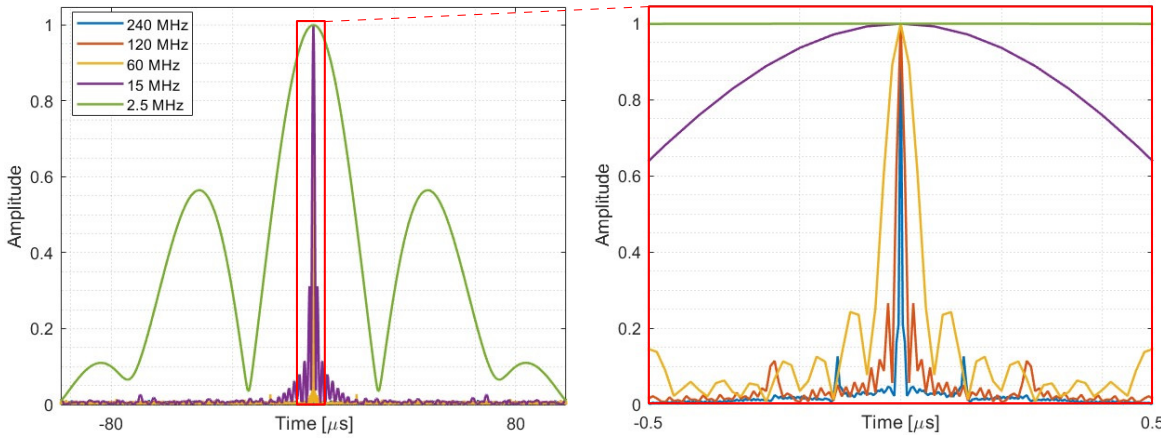

Figure 4: Auto-correlation profile of estimated beacon versus bandwidth.

IV. STARLINK SIGNAL ACQUISITION AND TRACKING

This section explains the acquisition stage and tracking loops used to track Starlink LEO SVs' Doppler without a high gain signal capture setup. All what follows assumes that M = 5 and F_s = 2.5 MHz to satisfy conditions (7) and (8). Let, K denote the accumulation index and $n \in \left[0, \frac{MT_{sub}}{Ts} - 1\right]$.

1. Acquisition

The acquisition stage follows the typical maximum likelihood estimator of the code phase $\hat{d}_K$ and $\hat{f}_{D,K}$, expressed as

$$[\hat{d}_K, \hat{f}_{D,K}] = \text{argmax}_{d,f_D} \left| \left(\hat{\mathbf{s}} \star \boldsymbol{r}_K^{\mathsf{T}} \exp[j2\pi f_D n T_s]\right)[d] \right|^2$$

It is noted that the granularity of the Doppler search space, call it Δf_D, should satisfy condition (7) such that maximum Doppler error is $\tilde{f}_D = \frac{\Delta f_D}{2}$ and the maximum Doppler rate error is $\tilde{\dot{f}}_D = 3$ kHz/s^2.

2. Kalman Filter Tracking

A KF approach is proposed to track both the code and carrier phase. Note that even though the estimated beacon is unambiguous, the resulting Doppler measurements will still contain an ambiguous Doppler shift term. This is because the LNB is expected to have nonzero frequency error at the time of data collection. This is the reason why the following tracking model will assume disjoint dynamics between the code phase and carrier phase. However, the ambiguity term can still be resolved by minimizing the error between the rate of the tracked code phase and the tracked Doppler after tracking is complete. Let $\boldsymbol{x}(t) \triangleq \left[\theta(t),\ \dot{\theta}(t),\ \ddot{\theta}(t),\ \tau(t),\ \dot{\tau}(t)\right]^{\mathsf{T}}$ be the state vector whose dynamics is modeled as $\dot{\boldsymbol{x}}(t) = \mathbf{A}\boldsymbol{x}(t) + \boldsymbol{w}(t)$,

$$\mathbf{A} \triangleq \begin{bmatrix} 0 & 1 & 0 & 0 & 0 \\ 0 & 0 & 1 & 0 & 0 \\ 0 & 0 & 0 & 0 & 0 \\ 0 & 0 & 0 & 0 & 1 \\ 0 & 0 & 0 & 0 & 0 \end{bmatrix},$$

where $\boldsymbol{w}(t)$ is a zero-mean white noise process with covariance matrix $\mathbf{Q} = \text{diag}\left[0, 0, (2\pi 0.2)^2, 0, 1\right]$. The discrete equivalent of the above model is $\boldsymbol{x}_{K+1} = \mathbf{F}\boldsymbol{x}_K + \boldsymbol{w}_K$, discretized at uniform intervals of MT_{sub} with $\boldsymbol{x}_K \triangleq \left[\theta_K,\ \dot{\theta}_K,\ \ddot{\theta}_K,\ d_K,\ \dot{d}_K\right]^{\mathsf{T}}$, where

$$\mathbf{F} = e^{\mathbf{A}MT_{sub}}, \quad \mathbf{Q}_d = \int_0^{MT_{sub}} e^{\mathbf{A}t}\mathbf{Q}\left(e^{\mathbf{A}t}\right)^{\mathsf{T}} dt,$$

such that $\mathbf{Q}_d$ is the covariance matrix of $\boldsymbol{w}_K$, which is the discrete-time equivalent of $\boldsymbol{w}(t)$. The observation model is $\boldsymbol{z}_K = \mathbf{C}\boldsymbol{x}_K + \boldsymbol{v}_K$ where,

$$\mathbf{C} \triangleq \begin{bmatrix} 0 & 1 & 0 & 0 & 0 \\ 0 & 0 & 0 & 1 & 0 \end{bmatrix}, \quad \boldsymbol{v}_k \sim \mathcal{N}\left(\begin{bmatrix} 0 \\ 0 \end{bmatrix}, \begin{bmatrix} \sigma_{\dot{\theta}}^2 & 0 \\ 0 & \sigma_{\tau}^2 \end{bmatrix}\right),$$

where the measurement noise variances $\sigma_{\dot{\theta}}^2$ and σ_{τ}^2 are set to $(2\pi 0.2)^2$ Hz^2 and 3.9 μs^2 respectively. Define the prompt, early, and late correlations in both time and frequency as

$$\begin{aligned} S^p(K) &= \left|\langle r_K[n], s[n]\rangle\right|^2 \\ S_t^e(K) &= \left|\langle r_K[n], s[n - B_t F_s]\rangle\right|^2 \\ S_t^l(K) &= \left|\langle r_K[n], s[n + B_t F_s]\rangle\right|^2 \\ S_f^e(K) &= \left|\langle r_K[n], s[n]\exp[-j2\pi B_f n T_s]\rangle\right|^2 \\ S_f^l(K) &= \left|\langle r_K[n], s[n]\exp[+j2\pi B_f n T_s]\rangle\right|^2, \end{aligned}$$

where term B_t is chosen to be 0.2 μs in accordance with the auto-correlation profile in Figure 4, and B_f is chosen to be 500 Hz to approximate the 3 dB bandwidth of the beacon correlation in the frequency-domain. Finally, the measurement pre-fit residual is defined as $\tilde{\boldsymbol{y}}_K = \left[\tilde{\dot{\theta}}_K,\ \tilde{d}_K\right]^{\mathsf{T}}$ where

$$\tilde{\dot{\theta}}_K = \frac{S_f^e(K) - S_f^l(k)}{S_f^e(K) + S_f^l(K)}, \quad \tilde{d}_K = \frac{S_t^e(K) - S_t^l(K)}{S_t^e(K) + S_t^l(K)}.$$

Note that without a high gain signal capture setup, the KF relies on non-zero user activity to remain in a locked state. However, as can be seen from Figure 3, the received signal power is non-stationary. Therefore, in intervals were no user activity is present, the KF must at least have a rough estimate of the Doppler rate and code phase rate. This is to allow the filter to propagate the dynamic model and remain in a locked state when frame activity returns. Define $\hat{\dot{\theta}}_K$ and $\hat{\dot{d}}_K$ as the estimates of the Doppler rate and code rate, respectively. Linear regression is used to estimate these variables from the last N KF estimates of d_K and

$\dot{\theta}_K$ that satisfy the condition $S^p(K) > \lambda$, where N and λ are both tunable parameters. These estimates allow continuous KF tracking with non-stationary user activity.

V. EXPERIMENTAL RESULTS

This section presents experimental tracking and positioning results that can be achieved with the presented framework. To this end a stationary NI-USRP X-410 was set to record the Starlink downlink channel from 4 different LNBs with the carrier frequency f_c set to 11.325 GHz, the sampling frequency F_s was set to 2.5 MHz, and the total recording duration was set to 1500 seconds. The LNBs were placed in a rhombus formation so that Starlink SV signals can be captured from all directions. Figure 5(a) shows the tracked Doppler versus TLE + SGP4 generated Doppler measurements.

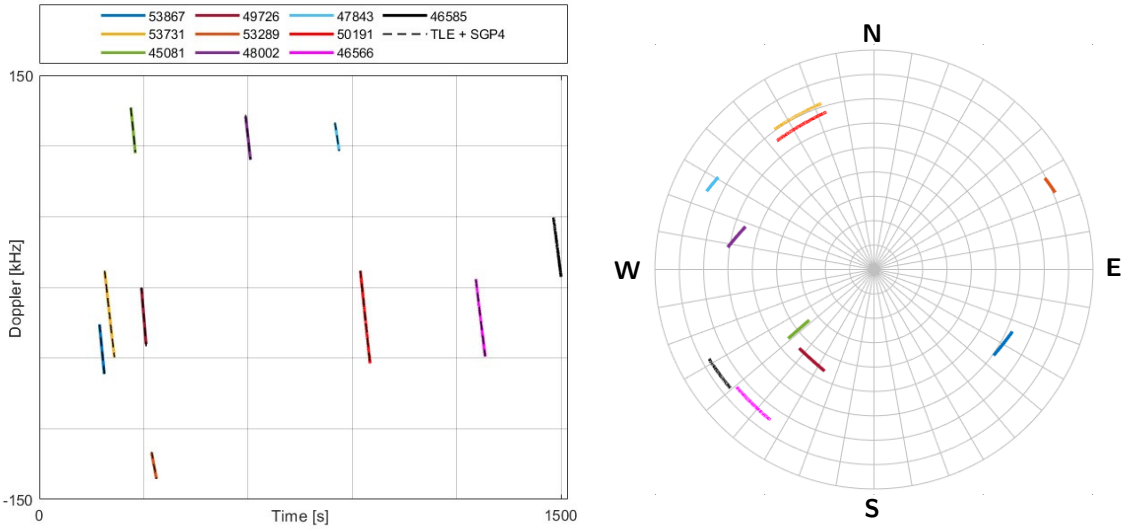

Figure 5: (a) Reciever tracked Doppler vs. TLE + SGP4 estimated Doppler.(b) Skyplot of tracked Starlink LEO SVs.

1. Measurement Model

The tracked Doppler measurements were integrated to generate carrier phase observables, calculated as

$$\Phi_s(K) \triangleq \frac{cMT_{sub}}{2\pi f_c} \sum_{i=0}^{K-1} \hat{\dot{\theta}}_i, \tag{9}$$

where $s \in [1, S]$ denotes the SV index, c is the speed-of-light, and S is the total number of tracked SVs. The carrier phase model is expressed as

$$\Phi_s(K) = \|\boldsymbol{r}_r - \boldsymbol{r}_s(K)\|_2 + \delta t_s(K) + N_s + v_s(K), \tag{10}$$

where $\boldsymbol{r}_r \triangleq [x_r, y_r, z_r]^\intercal$ is the receiver's 3D position; $\boldsymbol{r}_s \triangleq [x_s, y_s, z_s]^\intercal$ is the 3D position of the *s-th* SV; $\delta t_s(K)$ is a term modeling the lumped effects of clock errors and atmospheric delays; N_s is the carrier phase ambiguity of the *s-th* SV; v_s is the discrete-time measurement noise modeled as zero-mean white whose variance is derived from the estimation covariance of the KF. Note that in order to simplify the formulation of the nonlinear least-squares (NLS) filter, this model assumes that the signal time-of-flight has negligible effect on the SVs' positions and clock biases. Furthermore, $\delta_s(K)$ and N_s are lumped and approximated by their first-order TSE to rewrite (10) as

$$\Phi_s(K) \approx \|\boldsymbol{r}_r - \boldsymbol{r}_s(k)\|_2 + a_s + b_s K(MT_{sub}) + v_s(K),$$

where a_s and b_s are the zeroth- and first-order TSE coefficients.

2. Positioning Filter

Define a state vector $\boldsymbol{x} \triangleq \left[\boldsymbol{r}_r{}^{\mathsf{T}}, a_1, b_1, \ldots, a_S, b_S\right]^{\mathsf{T}}$ where the total number of tracked SVs is $S = 10$. Let, $\boldsymbol{\Phi}(K)$ denote the carrier phase measurements available from all S SVs at time instant K stacked into a column. Let, $\boldsymbol{z}$ denote the column vector containing $\boldsymbol{\Phi}(K)$ for every available K. Then, one can readily write the measurement model $\boldsymbol{z} = h(\boldsymbol{x}) + \boldsymbol{v}$ where $h(\boldsymbol{x})$ is a nonlinear vector function mapping the state space to the measurement space, and $\boldsymbol{v}$ is the measurement noise vector. At this point, the SV positions are propagated using TLE + SGP4. It is important to note that the TLE epoch time was adjusted such that it minimizes the range residuals for each SV to account for ephemeris timing errors. Finally, an NLS is used to estimate the stationary receivers true position. The solution results are shown in Figure 6. The initial position estimate was set 100 km away from the receiver's true position, and the final 2D error converged to within 21.2 m.

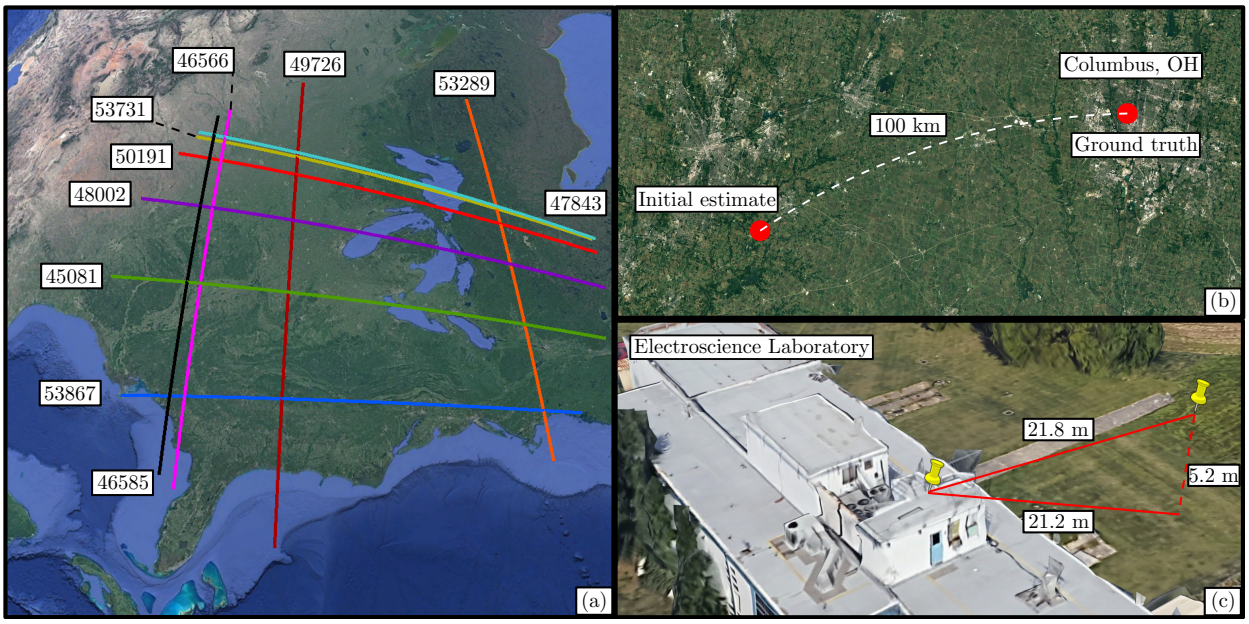

Figure 6: (a) Starlink LEO SVs' trajectories, (b) initial estimate distance from ground truth, and (c) final positioning solution and errors.

VI. CONCLUSION

This paper considered acquisition and tracking of Starlink LEO signals in low SNR regime, enabling exploitation of such signals for opportunistic PNT. Coherence conditions for which Starlink's signals can be blindly tracked in low SNR regime were derived. The full-bandwidth Starlink beacon was estimated, and a time-bandwidth analysis of this beacon was presented. A KF-based tracking loop was proposed for joint code and carrier phase tracking. Experimental results were presented showing successful Doppler tracking of 10 Starlink LEO SVs with a stationary receiver in low SNR regime. The Doppler observables were fused in a batch NLS estimator to yield a 2D positioning error of 21.2 m, starting from an initial estimate 100 km away from the receiver's true position.

ACKNOWLEDGMENTS

This work was supported in part by the Office of Naval Research (ONR) under Grants N00014-19-1-2511 and N00014-22-1-2242, in part by the Air Force Office of Scientific Research (AFOSR) under Grant FA9550-22-1-0476, and in part by the U.S. Department of Transportation (USDOT) under Grant 69A3552047138.

REFERENCES

3GPP (2010). Evolved universal terrestrial radio access (E-UTRA); multiplexing and channel coding. TS 36.212, 3rd Generation Partnership Project (3GPP).

3GPP (2018). Physical channels and modulation. TS 38.211, 5G; NR; 3rd Generation Partnership Project (3GPP).

3GPP2 (2011). Physical layer standard for cdma2000 spread spectrum systems (C.S0002-E). TS C.S0002-E, 3rd Generation Partnership Project 2 (3GPP2).

Bilardi, S. (2021). A GNSS signal simulator and processor for evaluating acquisition and tracking of GPS-like signals from satellites in LEO. Master's thesis, University of Colorado at Boulder, CO, USA.

Bolcskei, H. (2001). Blind estimation of symbol timing and carrier frequency offset in wireless OFDM systems. *IEEE Transactions on Communications*, 49(6):988–999.

Burel, G. and Bouder, C. (2000). Blind estimation of the pseudo-random sequence of a direct sequence spread spectrum signal. In *Proceedings of IEEE Military Communications Conference*, volume 2, pages 967–970.

Cassel, R., Scherer, D., Wilburne, D., Hirschauer, J., and Burke, J. (2022). Impact of improved oscillator stability on LEO-based satellite navigation. In *Proceedings of ION International Technical Meeting*, pages 893–905.

Chen, X., Wei, Q., Wang, F., Jun, Z., Wu, S., and Men, A. (2020). Super-resolution time of arrival estimation for a symbiotic FM radio data system. *IEEE Transactions on Broadcasting*, 66(4):847–856.

Chi, Y., Park, J., and Park, S. (2023). Hybrid multibeamforming receiver with high-precision beam steering for low Earth orbit satellite communication. *IEEE Transactions on Antennas and Propagation*, 71(7):5695–5707.

Choi, H. and Moon, H. (2020). Blind estimation of spreading sequence and data bits in direct-sequence spread spectrum communication systems. *IEEE Access*, 8:148066–148074.

del Peral-Rosado, J., Nolle, P., Rothmaier, F., Razavi, S., Lindmark, G., Jiang, X., Shrestha, D., Gunnarsson, F., Parsawar, S., Mundlamuri, R., Kaltenberger, F., Sirola, N., Sarkka, O., Noman, U., Rostrom, J., Vaarala, K., Miettinen, P., Garlaschi, S., Canzian, L., Babaroglu, H., Rastorgueva-Foi, E., Turunen, M., Talvitie, J., and Flachs, D. (2022). Proof-of-concept of dedicated aerial 5G and GNSS testbed for enhanced hybrid positioning. In *Proceedings of ION GNSS Conference*, pages 2362–2376.

Egea-Roca, D., Lopez-Salcedo, J., Seco-Granados, G., and Falletti, E. (2022). Performance analysis of a multi-slope chirp spread spectrum signal for PNT in a LEO constellation. In *Proceedings of Workshop on Satellite Navigation Technology*, pages 1–9.

Farhangian, F., Benzerrouk, H., and Landry, R. (2021). Opportunistic in-flight INS alignment using LEO satellites and a rotatory IMU platform. *Aerospace*, 8(10):280–281.

Fokin, G. and Volgushev, D. (2022). Software-defined radio network positioning technology design. problem statement. In *Proceedings of Systems of Signals Generating and Processing in the Field of on Board Communications*, pages 1–6.

Guo, F., Yang, Y., Ma, F., Liu, Y. Z. H., and Zhang, X. (2023). Instantaneous velocity determination and positioning using doppler shift from a LEO constellation. *Satellite Navigation*, 4:9–21.

Hartnett, M. (2022). Performance assessment of navigation using carrier Doppler measurements from multiple LEO constellations. Master's thesis, Air Force Institute of Technology, Ohio, USA.

Hendrickson, R. (1997). Globalstar for the military. In *Proceedings of IEEE Military Communications Conference*, volume 3, pages 1173–1178.

Huang, C., Qin, H., Zhao, C., and Liang, H. (2022). Phase - time method: Accurate Doppler measurement for Iridium NEXT signals. *IEEE Transactions on Aerospace and Electronic Systems*, 58(6):5954–5962.

Humphreys, T., Iannucci, P., Komodromos, Z., and Graff, A. (2023). Signal structure of the Starlink Ku-band downlink. *IEEE Transactions on Aerospace and Electronics Systems*. accepted.

Janssen, T., Koppert, A., Berkvens, R., and Weyn, M. (2023). A survey on IoT positioning leveraging LPWAN, GNSS and LEO-PNT. *IEEE Internet of Things Journal*, 10(13):11135–11159.

Jardak, N. and Adam, R. (2023). Practical use of Starlink downlink tones for positioning. *Sensors*, 23(6):3234–3253.

Jardak, N. and Jault, Q. (2022). The potential of LEO satellite-based opportunistic navigation for high dynamic applications. *Sensors*, 22(7):2541–2565.

Jiang, M., Qin, H., Su, Y., Li, F., and Mao, J. (2023). A design of differential-low Earth orbit opportunistically enhanced GNSS (D-LoeGNSS) navigation framework. *Remote Sensing*, 15(8):2136–2158.

Jiang, M., Qin, H., Zhao, C., and Sun, G. (2022). LEO Doppler-aided GNSS position estimation. *GPS Solutions*, 26(1):1–18.

Jiao, Z., Chen, L., Lu, X., Liu, Z., Zhou, X., Zhuang, Y., and Guo, G. (2023). Carrier phase ranging with DTMB signals for urban pedestrian localization and GNSS aiding. *Remote Sensing*, 15(2):423–446.

Kanamori, H., Kobayashi, K., and Kubo, N. (2023). A map-matching based positioning method using Doppler tracking and estimation by a software-defined receiver for multi-constellation LEO satellites. In *Proceedings of ION International Technical Meeting*, pages 649–663.

Kassas, Z., Kozhaya, S., Saroufim, J., Kanj, H., and Hayek, S. (2023). A look at the stars: Navigation with multi-constellation LEO satellite signals of opportunity. *Inside GNSS Magazine*, 18(4):38–47.

Kassas, Z., Morales, J., and Khalife, J. (2019). New-age satellite-based navigation – STAN: simultaneous tracking and navigation with LEO satellite signals. *Inside GNSS Magazine*, 14(4):56–65.

Kassas, Z., Neinavaie, M., Khalife, J., Khairallah, N., Haidar-Ahmad, J., Kozhaya, S., and Shadram, Z. (2021). Enter LEO on the GNSS stage: Navigation with Starlink satellites. *Inside GNSS Magazine*, 16(6):42–51.

Khalife, J., Neinavaie, M., and Kassas, Z. (2022). The first carrier phase tracking and positioning results with Starlink LEO satellite signals. *IEEE Transactions on Aerospace and Electronic Systems*, 56(2):1487–1491.

Khalife, J., Shamaei, K., and Kassas, Z. (2016). A software-defined receiver architecture for cellular CDMA-based navigation. In *Proceedings of IEEE/ION Position, Location, and Navigation Symposium*, pages 816–826.

Kozhaya, S., Kanj, H., and Kassas, Z. (2023). Multi-constellation blind beacon estimation, Doppler tracking, and opportunistic positioning with OneWeb, Starlink, Iridium NEXT, and Orbcomm LEO satellites. In *Proceedings of IEEE/ION Position, Location, and Navigation Symposium*, pages 1184–1195.

Kozhaya, S. and Kassas, Z. (2022). Blind receiver for LEO beacon estimation with application to UAV carrier phase differential navigation. In *Proceedings of ION GNSS Conference*, pages 2385–2397.

Kozhaya, S. and Kassas, Z. (2023). Positioning with Starlink LEO satellites: A blind Doppler spectral approach. In *Proceedings of IEEE Vehicular Technology Conference*, pages 1–5.

Li, L., Zhang, H., Du, S., Liang, T., and Gao, L. (2023). Blind despreading and deconvolution of asynchronous multiuser direct sequence spread spectrum signals under multipath channels. *IET Signal Processing*, 17(5):1–14.

Liu, W., Wang, J., and Li, S. (2010). Blind detection and estimation of OFDM signals in cognitive radio contexts. In *Proceedings of International Conference on Signal Processing Systems*, volume 2, pages 347–351.

Menzione, F. and Paonni, M. (2023). LEO-PNT mega-constellations: a new design driver for the next generation MEO GNSS space service volume and spaceborne receivers. In *Proceedings of IEEE/ION Position, Location, and Navigation Symposium*, pages 1196–1207.

Merwe, J., Bartl, S., O'Driscoll, C., Rügamer, A., Förster, F., Berglez, P., Popugaev, A., and Felber, W. (2020). GNSS sequence extraction and reuse for navigation. In *Proceedings of ION GNSS+ Conference*, pages 2731–2747.

More, H., Cianca, E., and Sanctis, M. (2022). Positioning performance of LEO mega constellations in deep urban canyon environments. In *Proceedings of International Symposium on Wireless Personal Multimedia Communications*, pages 256–260.

Mortlock, T. and Kassas, Z. (2021). Assessing machine learning for LEO satellite orbit determination in simultaneous tracking and navigation. In *Proceedings of IEEE Aerospace Conference*, pages 1–8.

Morton, Y., Xu, D., and Jiao, Y. (2022). Ionospheric scintillation effects on signals transmitted from LEO satellites. In *Proceedings of ION GNSS Conference*, pages 2980–2988.

Navstar GPS (2015). Space segment/navigation user interfaces interface specification IS-GPS-200. `http://www.gps.gov/technical/icwg/`.

Neinavaie, M. and Kassas, Z. (2022). Unveiling beamforming strategies of Starlink LEO satellites. In *Proceedings of ION GNSS Conference*, pages 2525–2531.

Neinavaie, M. and Kassas, Z. (2023a). Signal mode transition detection in Starlink leo satellite downlink signals. In *Proceedings of IEEE/ION Position, Location, and Navigation Symposium*, pages 360–364.

Neinavaie, M. and Kassas, Z. (2023b). Unveiling Starlink LEO satellite OFDM-like signal structure enabling precise positioning. *IEEE Transactions on Aerospace and Electronic Systems*. accepted.

Neinavaie, M., Khalife, J., and Kassas, Z. (2021). Blind Doppler tracking and beacon detection for opportunistic navigation with LEO satellite signals. In *Proceedings of IEEE Aerospace Conference*, pages 1–8.

Neinavaie, M., Khalife, J., and Kassas, Z. (2022). Acquisition, Doppler tracking, and positioning with Starlink LEO satellites: First results. *IEEE Transactions on Aerospace and Electronic Systems*, 58(3):2606–2610.

Pinell, C., Prol, F., Bhuiyan, M., and Praks, J. (2023). Receiver architectures for positioning with low earth orbit satellite signals: a survey. *EURASIP Journal on Advances in Signal Processing*, 2023:60–80.

Prol, F., Ferre, R., Saleem, Z., Välisuo, P., Pinell, C., Lohan, E., Elsanhoury, M., Elmusrati, M., Islam, S., Celikbilek, K., Selvan, K., Yliaho, J., Rutledge, K., Ojala, A., Ferranti, L., Praks, J., Bhuiyan, M., Kaasalainen, S., and Kuusniemi, H. (2022). Position, navigation, and timing (PNT) through low earth orbit (LEO) satellites: A survey on current status, challenges, and opportunities. *IEEE Access*, 10:83971–84002.

Prol, F., Kaasalainen, S., Lohan, E., Bhuiyan, M., Praks, J., and Kuusniemi, H. (2023). Simulations using LEO-PNT systems: A brief survey. In *Proceedings of IEEE/ION Position, Location, and Navigation Symposium*, pages 1381–387.

Raquet *et al.*, J. (2021). Position, navigation, and timing technologies in the 21st century. volume 2, Part D: Position, Navigation, and Timing Using Radio Signals-of-Opportunity, chapter 35–43, pages 1115–1412. Wiley-IEEE.

Rui, Z., Ouyang, X., Zeng, F., and Xu, X. (2022). Blind estimation of GPS M-Code signals under noncooperative conditions. *Wireless Communications and Mobile Computing*, 2022.

Sabbagh, R. and Kassas, Z. (2023). Observability analysis of receiver localization via pseudorange measurements from a single LEO satellite. *IEEE Control Systems Letters*, 7(3):571–576.

Saroufim, J., Hayek, S., and Kassas, Z. (2023). Simultaneous LEO satellite tracking and differential LEO-aided IMU navigation. In *Proceedings of IEEE/ION Position Location and Navigation Symposium*, pages 179–188.

Shi, C., Zhang, Y., and Li, Z. (2023). Revisiting Doppler positioning performance with LEO satellites. *GPS Solutions*, 27(3):126–137.

Singh, U., Shankar, M., and Ottersten, B. (2022). Opportunistic localization using LEO signals. In *Proceedings of Asilomar Conference on Signals, Systems, and Computers*, pages 894–899.

Souli, N., Kolios, P., and Ellinas, G. (2022). Online relative positioning of autonomous vehicles using signals of opportunity. *IEEE Transactions on Intelligent Vehicles*, 7(4):873–885.

Stock, W., Hofmann, C., and Knopp, A. (2023). LEO-PNT with Starlink: Development of a burst detection algorithm based on signal measurements. In *Proceedings of International ITG Workshop on Smart Antennas and Conference on Systems, Communications, and Coding*, pages 1–6.

Tan, Z., Qin, H., Cong, L., and Zhao, C. (2019). Positioning using IRIDIUM satellite signals of opportunity in weak signal environment. *Electronics*, 9(1):37.

Tanda, M. (2004). Blind symbol-timing and frequency-offset estimation in OFDM systems with real data symbols. *IEEE Transactions on Communications*, 52(10):1609–1612.

Tian, J., Fangchi, L., Yafei, T., and Dongmei, L. (2023). Utilization of non-coherent accumulation for LTE TOA estimation in weak LOS signal environments. *EURASIP Journal on Wireless Communications and Networking*, 2023(1):1–31.

Tsatsanis, M. and Giannakis, G. (1997). Blind estimation of direct sequence spread spectrum signals in multipath. *IEEE Transactions on Signal Processing*, 45(5):1241–1252.

Wang, D., Qin, H., and Huang, Z. (2023). Doppler positioning of LEO satellites based on orbit error compensation and weighting. *IEEE Transactions on Instrumentation and Measurement*, 72:1–11.

Wei, Q., Chen, X., and Zhan, Y. (2020). Exploring implicit pilots for precise estimation of LEO satellite downlink Doppler frequency. *IEEE Communications Letters*, 24(10):2270–2274.

Wu, N., Qin, H., and Zhao, C. (2023). Long-baseline differential doppler positioning using space-based SOP based on BPVGMM. *IEEE Transactions on Instrumentation and Measurement*, 72:1–10.

Yang, C. and Soloviev, A. (2023). Starlink Doppler and Doppler rate estimation via coherent combining of multiple tones for opportunistic positioning. In *Proceedings of IEEE/ION Position, Location, and Navigation Symposium*, pages 1143–1153.

Yang, C., Zang, B., Gu, B., Zhang, L., Dai, C., Long, L., Zhang, Z., Ding, L., and Ji, H. (2023). Doppler positioning of dynamic targets with unknown LEO satellite signals. *Electronics*, 12(11):2392–2404.

Ye, L., Gao, N., Yang, Y., Deng, L., and Li, H. (2023). Three satellites dynamic switching range integrated navigation and positioning algorithm with clock bias cancellation and altimeter assistance. *Aerospace*, 10(5):411–438.

Zhao, C., Qin, H., Wu, N., and Wang, D. (2023). Analysis of baseline impact on differential doppler positioning and performance improvement method for LEO opportunistic navigation. *IEEE Transactions on Instrumentation and Measurement*, 72:1–10.